Nonlinear solutions for $\chi^{(2)}$ frequency combs in optical microresonators

E. Podivilov,[1,2] S. Smirnov,[2] I. Breunig,[3,4] and B. Sturman[1]

[1]*Institute of Automation and Electrometry, Russian Academy of Sciences, 630090 Novosibirsk, Russia*

[2]*Novosibirsk State University, 630090, Novosibirsk, Russia*

[3]*University of Freiburg, Georges-Köhler-Allee 102, D-79110 Freiburg, Germany*

[4]*Fraunhofer Institute for Physical Measurement Techniques, D-79110 Freiburg, Germany*

(Received 9 October 2019; accepted 13 January 2020; published 11 February 2020)

Experimental and theoretical studies of nonlinear frequency combs in $\chi^{(3)}$ optical microresonators attracted tremendous research interest during the last decade and resulted in prototypes of soliton-based steadily working devices. Realization of similar combs owing to $\chi^{(2)}$ optical nonlinearity promises new breakthroughs and is a big scientific challenge. We analyze the main obstacles for realization of the $\chi^{(2)}$ frequency combs in high-Q microresonators and propose two families of steady-state nonlinear solutions, including soliton and periodic solutions, for such combs. Despite periodicity of light fields inside microresonators, the nonlinear solutions can be topologically different and relevant to periodic and antiperiodic boundary conditions. The antiperiodic states are expected to be the most favorable for the comb generation. The found particular solutions exist owing to a large difference in the group velocities between the first and second harmonics, typical of $\chi^{(2)}$ microresonators, and to the presence of the pump. They have no zero-pump counterparts relevant to conservative solitons. The stability issue for the found comb solutions remains open and requires further numerical analysis.

DOI: 10.1103/PhysRevA.101.023815

I. INTRODUCTION

Optical microresonators are the subject of numerous experimental and theoretical studies during the last two decades, as reviewed in [1–5]. Ultrahigh (up to 10^{11}) quality factors of the modes, quasidiscrete modal structure, and strong enhancement of the light intensity inside owing to the resonant recirculation are distinctive features of the case. Both $\chi^{(3)}$ and $\chi^{(2)}$ optical materials (amorphous and crystalline) can be employed. Numerous techniques for engineering of the modal frequency spectrum and coupling light in and out are well developed. Applications of microresonators range from sensors of single atoms and molecules to nonlinear optics. The latter strongly benefit from the possibility to use low-power continuous-wave light sources.

One of the most spectacular achievements in the nonlinear optics of microresonators based on $\chi^{(3)}$ materials is generation of broad high-quality frequency combs; see [6–15] and references therein. It took about one decade to proceed from the first observations and interpretations to the final concept of solitons and its realization on different platforms [15]. According to this concept, the most advanced combs are a manifestation of spatially narrow solitons circulating along the resonator rim with a constant velocity. The solitons in question are dissipative solitons with a double balance between (i) dispersion broadening and nonlinear narrowing and (ii) between an external pumping and dissipative losses [15]. It turned out that such solitons are stable against small perturbations. They are essentially different from (and more complicated than) the so-called conservative solitons existing without pumping and dissipation [16].

Application of the soliton concept of frequency combs to microresonators based on $\chi^{(2)}$ materials represents a big scientific challenge and, simultaneously, a highly perspective field. It promises employment of lower light powers, of different spectral ranges, and of new operation regimes. The problem encountered has a certain basis in the previous studies of conservative $\chi^{(2)}$ spatial and temporal solitons employing cascading processes of second-harmonic generation and optical parametric oscillation; see review [17] and references therein. This basis is, however, insufficient because of (i) incompleteness of knowledge in the field of conservative solitons, (ii) the necessity of transfer to dissipative solitons, and (iii) the necessity to incorporate specific features of nonlinear optics of microresonators. First models for $\chi^{(2)}$ solitons in microresonators were published recently [18–20]. Attempts to explore $\chi^{(2)}$ frequency combs regardless of solitons are reported in [21–24]. In particular, walk-off controlled domain-wall-like comb solutions were proposed [25]. Also, the so-called simulton-solitons are reported recently for meter-scale parametric oscillators [26]. The area remains, in essence, largely unexplored.

The following features specific for the $\chi^{(2)}$ frequency combs have to be indicated.

(1) The first and second harmonics (FH and SH) in $\chi^{(2)}$ materials are not phase matched in the general case, so that their nonlinear coupling is negligible except for special cases. The quasi-phase-matching employing proper radial poling of microresonators [27,28] has to be used to overcome this problem. Properties of the radial poling have to be special for each operation regime.

(2) The group velocities of FH and SH are generally different, so that the corresponding wave envelopes separate from each other unless the nonlinear coupling compensates for this separation. The effect of the group velocity difference is typically very strong and dominating over the effects of

frequency dispersion. Very little is known about dispersionless soliton regimes.

(3) In the cases when the quasi-phase-matching is combined with a zero group velocity difference and the effects of frequency dispersion are important, the signs of the frequency dispersion are typically opposite for FH and SH. This imposes additional restrictions on the soliton regimes.

(4) There are two principal cases for generation of $\chi^{(2)}$ frequency combs—pumping into FH and SH modes. In the first case, primarily pumped monochromatic FH excites a SH, which can be unstable against generation of side FHs. Here, the spatially uniform background states for FH and SH exist and represent an important ingredient of soliton physics. In the second case of pumped SH, the spatially uniform FH and SH backgrounds do not necessarily exist leading to specific comb generation regimes.

In this paper, we focus on the case of SH pumping and the dominating effect of the group velocity difference. At the same time, our basic equations incorporate the effects of frequency dispersion. As in the previous approaches to comb modeling, we assume that each resonator mode can be characterized by a single modal number. This assumption can be implemented by proper shaping of the resonator rim. It strongly simplifies the considerations.

II. BASIC EQUATIONS

The light modes (whispering gallery modes) can be viewed as quasi-one-dimensional waves, with wave vectors $k_j = j/R$ and very large ($\sim 10^4$) integer azimuth mode number j, propagating along the rim of an axisymmetric resonator with big radius R; see Fig. 1(a).

The modal light fields depend on the azimuth angle φ as $\exp(ij\varphi)$. Details of localization of light fields near the rim for the chosen modes are of minor importance for this study. The modal frequencies are discrete and given by $\omega_j = k_j c/n_j$, where c is the speed of light and n_j is the modal refractive index. Frequency ω_j corresponds to the vacuum wavelength $\lambda_j = 2\pi c/\omega_j$, and the modal refractive index can be treated as a smooth function $n(\lambda)$ to characterize the modal group velocity and dispersion. For $\chi^{(2)}$ resonators, radius R is typically of the order of 1 mm. Here, the smooth function $n(\lambda)$ is close to the function $n_0(\lambda)$ characterizing the bulk material. Small corrections $n - n_0$ are size and shape dependent [29–31] and can be taken into account for application to particular resonators. Generally, two polarization types of modes, with different dependencies $n(\lambda)$, exist in microresonators.

In the case of azimuth symmetry, the phase-matching condition for SH generation is $2\omega_j = \omega_{2j}$. It is valid also for parametric generation of mode j by mode with the azimuth number $2j$. Except for special cases, this phase-matching condition cannot be fulfilled [32]. Moreover, the frequency distance $2\omega_j - \omega_{2j}$, being much smaller than ω_j, is usually much larger than the intermodal distance $\delta\omega = c/nR$.

Periodic radial poling is in use to provide phase matching in a designated spectral range [27,28]. It is illustrated by Figs. 1(b)–1(d). Ideally, the radial poling does not influence the linear optical properties and results in a strictly periodic φ alternation of the sign of the quadratic susceptibility coefficient d, as indicated in Fig. 1(c). If N is the number of

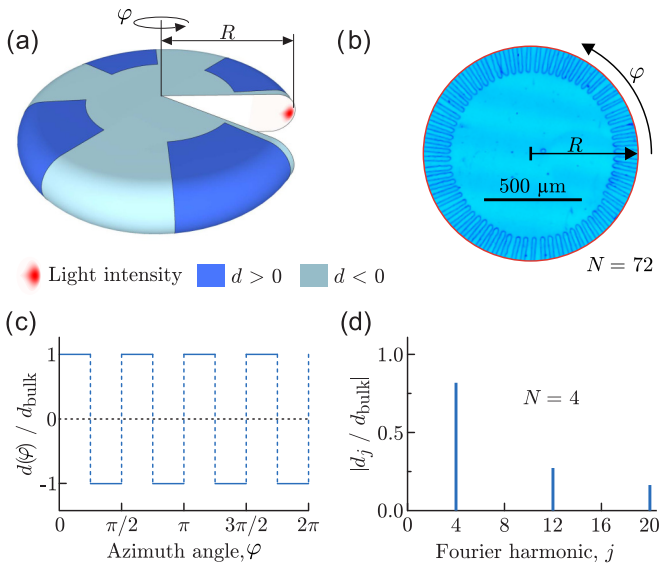

FIG. 1. Resonator geometry and radial poling. (a) Resonator shape and cross section; φ is the azimuth angle; the major radius R is different from the rim curvature radius. The red spot shows localization of light, and different colors indicate the radial poling. (b) Micrograph of radially poled lithium-niobate-based resonator with the number of domain periods $N = 72$. (c) Schematic of the azimuth dependence of the nonlinear coefficient $d(\varphi)$ for perfectly periodic poling with $N = 4$. (d) First harmonics of the Fourier spectrum $|d_j|$ for (c).

alternation periods, the azimuth dependence $d(\varphi)$ is given by the Fourier series $d = d_0 + d_1 \exp(iN\varphi) + d_3 \exp(3iN\varphi) + \ldots$, where $|d_1|$ can be comparable with the bulk value of d [27]. The Fourier spectrum of $d(\varphi)$ for the perfect poling is illustrated by Fig. 1(d). The higher peaks are typically unimportant for phase matching. The phase-matching condition for SH generation reads now $2\omega_j = \omega_{2j\pm N}$, where the sign "plus" is relevant to the most typical case of decreasing $n(\lambda)$. By choosing N, it can be fulfilled with a good accuracy (within the intermodal distance) for any j. Modification of the phase-matching conditions for generation of sum and difference frequencies can be made similarly.

Now, we write down generic nonlinear equations for complex modal amplitudes F_j and S_l relevant to the FH and SH frequency domains and the phase-matching condition $2\omega_j = \omega_{2j+N}$. Assuming pumping into a SH mode with modal number l_0, we have

$$
\begin{aligned}
i\dot{F}_j - (\omega_j - i\gamma_j)F_j &= 2\mu \sum_{l,j'} S_l F_{j'}^* \, \delta_{l-j-j'-N}, \\
i\dot{S}_l - (\omega_l - i\gamma_l)S_l &= \mu \sum_{j,j'} F_j F_{j'}' \delta_{l-j-j'-N} + ih\delta_{l-l_0} e^{-i\omega_p t}.
\end{aligned}
\tag{1}
$$

Here the dot indicates differentiation in time t, $\gamma_{j,l}$ are the modal decay constants, such that the quality factor is $Q_j = \omega_j/2\gamma_j \gg 1$, μ is a coupling coefficient incorporating the relevant susceptibility coefficient and modal overlaps [3,33], ω_p is the pump frequency, h is a variable parameter characterizing pump strength, and the asterisk indicates complex

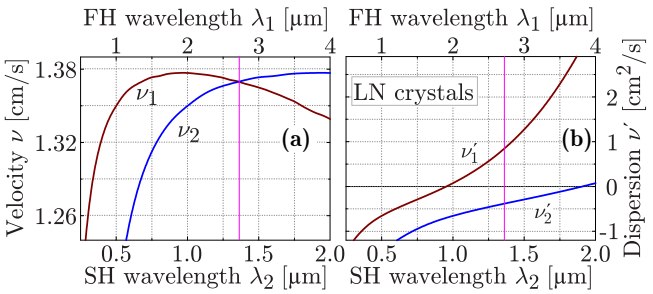

FIG. 2. Wavelength dependencies of $v_{1,2}$ (a) and $v'_{1,2}$ (b) for $LiNbO_3$ crystals with the geometric dispersion neglected. The vertical line corresponds to the case $v_1 = v_2$, where $v'_1 v'_2 < 0$.

conjugation. The amplitudes are normalized such that $\omega_j |F_j|^2$ and $\omega_l |S_l|^2$ are the modal energies. Without loss of generality, μ and h can be treated as real positive quantities. The modes F and S can be polarizationally the same or different. The case $N = 0$ corresponds to phase matching of differently polarized modes without radial poling [34]. Transfer to the case of FH pumping is evident. Note that the presence of a factor of 2 in Eq. (1) reflects the Hamiltonian nature of $\chi^{(2)}$ interactions in the absence of dissipation.

Further simplifications involve an assumption of relative narrowness of the FH and SH spectra. Let the numbers j and l be close to j_0 and l_0, respectively, so that the deviations $\delta j = j - j_0$ and $\delta l = l - l_0$ are much smaller than j_0 and l_0 in absolute values. Then we can employ expansions,

$$\omega_j = \omega_{j_0} + \nu_1 (j - j_0) + \alpha_1 (j - j_0)^2,$$
$$\omega_l = \omega_{l_0} + \nu_2 (l - l_0) + \alpha_2 (l - l_0)^2, \tag{2}$$

where $\nu = v/R$, $\alpha = v'/2R^2$, $v = d\omega_k/dk$ is the group velocity, $v' = dv/dk = d^2\omega_k/dk^2$ is the dispersion parameter, and indices 1 and 2 refer to $k_1 = j_0/R$ and $k_2 = l_0/R$. Parameters v and v' are fully determined by the dependence $n(\lambda)$.

Figure 2 shows representative wavelength dependencies of $v_{1,2}$ and $v'_{1,2}$ for $LiNbO_3$ crystals relevant to the bulk value $n_0(\lambda)$ and extraordinary polarization [35,36]. They show that the velocity difference $v_1 - v_2$ ranges from 0 to $\approx 10^{-2} c$, it can be positive and negative. The dispersion parameters can be of the same and opposite signs, they turn to zero at certain wavelengths. Influence of the resonator shape and size is minor for $R \sim 1$ mm. The mentioned features are crucial for the subsequent analysis of nonlinear comb solutions.

III. PERIODIC AND ANTIPERIODIC SOLUTIONS

Here we show that in the case of SH pumping there are two topologically different types of physical solutions for the FH and SH slowly varying amplitudes (envelopes) $F(\varphi, t)$ and $S(\varphi, t)$—the periodic and antiperiodic solutions. They obey the same fundamental set of coupled nonlinear equations and differ only in the boundary conditions. The periodic and antiperiodic solutions are relevant to pumping into SH modes with even and odd numbers $l_0 - N$, respectively.

Periodic solutions. Let the integer $l_0 - N$ be *even*. Then ω_{l_0} is close to $2\omega_{j_0}$ with $j_0 = (l_0 - N)/2$, so that the frequency mismatch $\Delta_0 = 2\omega_{j_0} - \omega_{l_0}$ is smaller in the absolute value than the intermodal distance $\delta\omega = c/nR$. It is convenient here to use the discrete deviations $\delta j = j - j_0$ and $\delta l = l - l_0$. The envelopes $F(\varphi, t)$ and $S(\varphi, t)$ are linked to $F_{\delta j}$ and $S_{\delta l}$ by the relations of discrete Fourier transform,

$$F = e^{i(\omega_{j_0} - \Delta_1)t} \sum_{\delta j} F_{j_0 + \delta j} e^{i\delta j \varphi},$$
$$S = e^{i(\omega_{l_0} - \Delta_2)t} \sum_{\delta l} S_{l_0 + \delta l} e^{i\delta l \varphi}, \tag{3}$$

where $\Delta_1 = (2\omega_{j_0} - \omega_p)/2$ and $\Delta_2 = \Delta_p = \omega_{l_0} - \omega_p$. To get equations for F and S, it is necessary to multiply the first and second of Eq. (1) by $\exp(i\delta j\varphi)$ and $\exp(i\delta l\varphi)$, respectively, take sums in δj and δl, and employ Eqs. (2) and (3) and the Kronecker symbols. Finally, we obtain

$$\hat{L}_1 F = 2\mu S F^*, \quad \hat{L}_2 S = \mu F^2 + ih, \tag{4}$$

where the linear differential operators $\hat{L}_{1,2}$ are given by

$$\hat{L}_{1,2} = i(\partial_t + \nu_{1,2}\partial_\varphi) + \alpha_{1,2}\partial_\varphi^2 - \Omega_{1,2}, \tag{5}$$

with $\Omega_{1,2} = \Delta_{1,2} - i\gamma_{1,2}$. The ν and α terms correspond to the effects of drift and dispersion of wave envelopes, respectively. These effects are generally substantially different for FH and SH amplitudes. For simplicity, we have neglected the wavelength dependencies of small damping coefficients $\gamma_{1,2}$. According to the definition (3), the amplitudes $F(\varphi, t)$, $S(\varphi, t)$ obey 2π-periodic boundary conditions: $F(\varphi \pm 2\pi, t) = F(\varphi, t)$, $S(\varphi \pm 2\pi, t) = S(\varphi, t)$. Detunings Δ_1 and Δ_2 have different meaning. The pump detuning Δ_2 can be easily tuned in experiment, while detuning Δ_1 is greatly determined by the material and resonator properties, it can be affected, e.g., by temperature tuning.

Remarkably, Eq. (4) possess spatially uniform steady-state solutions $\bar{F}$, $\bar{S}$; they are important for analysis of soliton solutions. Below the threshold of parametric instability, $h < h_{\text{th}} = |\Omega_1 \Omega_2|/2\mu$, we have a trivial solution $\bar{F} = 0$ and $\bar{S} = -ih/\Omega_2$. For $\bar{F} \neq 0$, we obtain $|\bar{S}| = h_{\text{th}}/|\Omega_2| = |\Omega_1|/2\mu$ and

$$\frac{2\mu^2 |\bar{F}|_\pm^2}{|\Omega_1 \Omega_2|} = \cos\Phi \pm \sqrt{\eta^2 - \sin^2\Phi}, \tag{6}$$

where $\eta = h/h_{\text{th}} = 2\mu h/|\Omega_1 \Omega_2|$ is the normalized pump strength and $\Phi = \arg(\Omega_1 \Omega_2)$.

Figure 3 illustrates the dependencies $|F_\pm|^2(\eta, \Phi) \neq 0$. For $0 \leqslant |\Phi| < \pi/2$, there are two branches, while for $\pi/2 \leqslant |\Phi| \leqslant \pi$ there is only a single branch. For $|\Phi| \ll 1$, the minimum value of η is $\eta_{\min} \simeq |\Phi|$. The branches $\bar{F}_-(\eta)$, with negative slopes, are expected to be unstable against spatially uniform and quasiuniform temporal perturbations; see also below. This means the presence of bistable background solutions for $\eta < 1$, $|\Phi| < \pi/2$ and, possibly, hysteresis when adiabatically increasing and decreasing η. The F_+ branches are stable against spatially uniform and quasiuniform temporal perturbations.

Antiperiodic solutions. Let now the integer $l_0 - N$ be *odd*. It cannot be equal to a double integer $2j_0$. In other words, the l_0 mode is coupled not to a single FH mode, but to two FH modes. The phase-matching conditions say here that $l_0 - N = 2j_0 + 1$ and ω_{l_0} is very close to $\omega_{j_0} + \omega_{j_0+1}$. Our goal is to introduce slowly varying amplitudes $F(\varphi, t)$ and

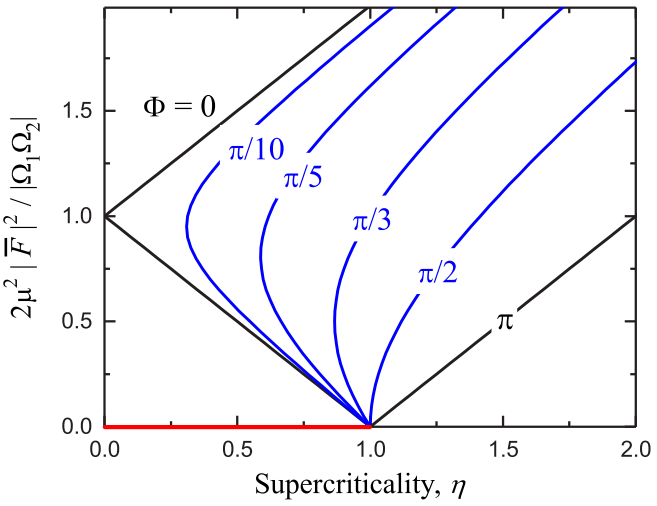

FIG. 3. Dependencies $|\bar{F}_\pm|^2(\eta)$ for different values of $\Phi = \arg(\Omega_1\Omega_2)$. The $\pm$ branches correspond to positive and negative slopes. The two-branch black curve with $\Phi = 0$ corresponds to the limiting case $\gamma_{1,2} \to 0$ at $\Delta_1\Delta_2 > 0$, while the black line $\Phi = \pi$ is relevant to the liming case $\gamma_{1,2} \to 0$ at $\Delta_1\Delta_2 < 0$ and to the case $\Delta_1 = \Delta_2 = 0$. The red segment shows the branch $\bar{F} = 0$ for $\bar{S} \neq 0$.

$S(\varphi, t)$ obeying again Eqs. (4) and (5). This can be done with expressions $F = \tilde{F}\exp(-i\varphi/2)$,

$$\tilde{F} = e^{i(\omega_{j_0} - \Delta_1 + \delta\omega_1/2)t} \sum_{\delta j} F_{j_0+\delta j}\, e^{i\delta j\varphi},$$

$$S = e^{i(\omega_{l_0} - \Delta_2)t} \sum_{\delta l} S_{l_0+\delta l}\, e^{i\delta l\varphi}, \tag{7}$$

where $\Delta_1 = (\omega_{j_0} + \omega_{j_0+1} - \omega_p)/2$ and, as earlier, $\Delta_2 = \Delta_p = \omega_{l_0} - \omega_p$. Here, the most remarkable feature is the presence of factor $\exp(-i\varphi/2)$ in the definition of F. Owing to this factor, the amplitude $F(\varphi, t)$ is 2π *antiperiodic*, $F(\varphi \pm 2\pi, t) = -F(\varphi, t)$, whereas the amplitude $S(\varphi, t)$ is again 2π periodic.

Note that the FH amplitude $\tilde{F}(\varphi, t)$, which differs from $F(\varphi, t)$ by a factor of $\exp(i\varphi/2)$, remains 2π periodic. Employment of the pair of amplitudes $\tilde{F}$, S leads us to the set,

$$\hat{L}_1'\tilde{F} = 2\mu S\tilde{F}^* e^{i\varphi}, \quad \hat{L}_2 S = \mu\tilde{F}^2 e^{-i\varphi} + ih, \tag{8}$$

where operator $\hat{L}_1'$ is different from $\hat{L}_1$ [see Eq. (5)], by the replacement $\Delta_1 \to \Delta_1' = \Delta_1 - \delta\omega_1/2$. In contrast to set (4), it includes 2π-periodic factors $\exp(\pm i\varphi)$ in the right-hand sides. This is inconvenient for analytical treatments but useful for numerical calculations.

The set of nonlinear equations (4) is thus quite general; it is valid for both the periodic and antiperiodic physical solutions. The same set serves also as the staring point of many $\chi^{(2)}$ comb studies; see, e.g., [18–20] and references therein. Lastly, it can be considered as a generalization of the conservative equations for $\chi^{(2)}$ solitons [17]. In essence, set (4) plays the role of the nonlinear Schrödinger equation supplemented by driving and decay terms (the so-called LL equation [10,37–39]) for the $\chi^{(3)}$ combs. However, set (4) is much more complicated and much less investigated compared to the LL equation. In particular, no attention was paid to the fact that the antiperiodic comb solutions of this set can be physical and relevant to the excitation of the SH modes with odd azimuth numbers.

The antiperiodic solutions (states) are topologically different from the conventional periodic states. No temporal evolution can make conversion between these two states. In contrast to the periodic states, the antiperiodic ones have no spatially uniform background. The schemes of nonlinear generation of FH and SH harmonics are also fundamentally different: The primary FH harmonics F_{j_0} and F_{j_0+1} not only influence the SH harmonic S_{l_0}, but induce immediately the side harmonics $S_{l_0\pm1}$. Generally, not only parametric, but also nonlinear driving terms for FH harmonics are present in the antiperiodic case. For this reason, broad FH and SH spectra appear above a single parametric oscillation threshold; see also Sec. V. This is why the antiperiodic states have advantages over the periodic states for the comb generation. Note finally that the notion of antiperiodic solutions is not applicable to the $\chi^{(3)}$ case.

IV. STEADY-STATE SOLUTIONS

A. General properties

Steady-state nonlinear solutions, where the FH and SH envelopes propagate with the same velocity, are of our prime interest. For such a solution we have $F(\varphi, t) = F(\tilde{\varphi})$ and $S(\varphi, t) = S(\tilde{\varphi})$, where $\tilde{\varphi} = \varphi - \nu_0 t$ is the moving frame coordinate, and ν_0 is a common angular velocity. This angular velocity corresponds to the linear velocity $v_0 = \nu_0 R$. We are interested in solutions strongly localized in $\tilde{\varphi}$.

In the case of even $l_0 - N$, the 2π-periodic amplitudes $F(\tilde{\varphi})$ and $S(\tilde{\varphi})$ can be expanded in Fourier series,

$$F = \sum_j F_j\, e^{ij\tilde{\varphi}}, \quad S = \sum_l S_l\, e^{il\tilde{\varphi}}. \tag{9}$$

This means that the frequency spectra of F and S consist of equidistant peaks separated by the same distance $\nu_0 = v_0/R$, i.e., we have a frequency comb. The smaller the scale of localization of $F(\tilde{\varphi})$ and $S(\tilde{\varphi})$, the broader is this comb. Note that positions of the equidistant frequency peaks cannot coincide with nonequidistant modal frequencies. This means that nonlinear frequency shifts must be involved in formation of the steady states.

In the case of odd $l_0 - N$, when $S(\tilde{\varphi})$ is 2π periodic and $F(\tilde{\varphi})$ is 2π antiperiodic, we must multiply F by the factor of $\exp(i\tilde{\varphi}/2)$ to get true 2π-periodic $\tilde{\varphi}$ dependence of the FH amplitude. This leads us again to a slightly different frequency comb with the frequency separation ν_0.

Importantly, velocity v_0 (or the angular frequency ν_0) cannot be chosen arbitrarily. It has to be determined simultaneously with nonlinear solution for $F(\tilde{\varphi})$ and $S(\tilde{\varphi})$. It can be different for the periodic and antiperiodic solutions.

As follows from Eqs. (4) and (5), the steady-state amplitudes $F(\tilde{\varphi})$ and $S(\tilde{\varphi})$ obey the set of nonlinear ordinary differential equations,

$$\left(i\nu_1^0\partial_{\tilde{\varphi}} + \alpha_1\partial_{\tilde{\varphi}}^2 - \Omega_1\right)F = 2\mu SF^*,$$
$$\left(i\nu_2^0\partial_{\tilde{\varphi}} + \alpha_2\partial_{\tilde{\varphi}}^2 - \Omega_2\right)S = \mu F^2 + ih, \tag{10}$$

where $\nu^0_{1,2} = \nu_{1,2} - \nu_0$. They have to be solved with 2π periodic and antiperiodic boundary conditions. The ν terms account for drift of F and S with different velocities, while the α terms are relevant to the effects of dispersion. The limit $\gamma_{1,2} \to 0$, when $\Omega_{1,2} = \Delta_{1,2}$, corresponds to the absence of dissipation. Generally, nonlinear set (10) with two complex amplitudes and several variable parameters, including velocity v_0, is much more complicated compared to the single equation describing the $\chi^{(3)}$ combs.

While we do not know velocity v_0 for nonlinear solutions, it is likely that it lies in between v_1 and v_2. Setting $|\nu^0_1| \approx |\nu^0_2| \approx |v_1 - v_2|/2R$, $|\alpha_1| \approx |\alpha_2| \approx |v'|/2R^2$, and assuming that $\delta\tilde{\varphi} \ll 2\pi$ is the scale of localization of $F(\tilde{\varphi})$ and $S(\tilde{\varphi})$, we can estimate the ratio of the drift to dispersion terms. It is about $|v_1 - v_2|R\delta\tilde{\varphi}/|v'|$. Adopting parameters of Fig. 2, we see that, except for the close vicinity of the point of equal group velocities, we have $|v_1 - v_2| \gtrsim 10^8$ cm/s and $|v'| \approx 10^4\,\mathrm{cm}^2/\mathrm{s}$. For $R \approx 1$ mm, this gives the ratio $\gtrsim 10^3/\delta\tilde{\varphi}$. Thus, for $\delta\tilde{\varphi} \gtrsim 10^{-3}$, which means the number of comb peaks $\lesssim 10^3$, the drift terms are dominating, and the dispersion terms can be omitted in the leading approximation. In order to omit the drift terms, we must stay practically at the point $v_1(\lambda_p) = v_2(\lambda_p)$. Slight deviations from this point switch the strong drift terms on. This situation is generic for $\chi^{(2)}$ resonators.

Note that the zero point of the frame coordinate $\tilde{\varphi}$ (and of the polar angle φ) can be chosen arbitrary. If $f(\tilde{\varphi})$, $s(\tilde{\varphi})$ is a particular steady-state solution, then $f(\tilde{\varphi} - \varphi_0)$, $s(\tilde{\varphi} - \varphi_0)$ with an arbitrary φ_0 is an equivalent solution. This degeneracy in φ_0 can be crucial for analysis of corrections to the primary steady states caused by various small perturbations, such as weak dissipation and dispersion.

B. Dispersionless solitons and periodic states

Here we demonstrate the possibility of different soliton solutions with the dissipative and dispersive terms neglected. To do so, we put $\alpha_{1,2} = \gamma_{1,2} = 0$ and set

$$v_0 = (2\Delta_1 v_2 + \Delta_2 v_1)/(2\Delta_1 + \Delta_2). \tag{11}$$

This common propagation velocity lies inside the interval $[v_1, v_2]$ for $\Delta_1\Delta_2 > 0$ and outside this interval for $\Delta_1\Delta_2 < 0$. Furthermore, we change from $\tilde{\varphi}$, F, and S to the normalized quantities $\zeta = R(2\Delta_1 + \Delta_2)\tilde{\varphi}/(v_2 - v_1)$, $f = \mu(2/|\Delta_1\Delta_2|)^{1/2}F$, and $s = -2\mu S/\Delta_1$. After that we have from Eq. (10),

$$\begin{aligned} i\dot{u} - u + s|u| &= 0, \\ i\dot{s} + s - qu &= \eta, \end{aligned} \tag{12}$$

where, as earlier, $\eta = 2|\mu h/\Delta_1\Delta_2|$ is the normalized pump strength, $u = f^2$, the dot indicates differentiation in ζ, and $q = \mathrm{sgn}(\Delta_1\Delta_2) = \pm 1$. The spatially uniform background values of s and u in our case are as follows (compare to Fig. 3): $\bar{s}_\pm = \mp 1$, $\bar{u}_\pm = \mp 1 - \eta$ for $q = 1$ ($\Phi = 0$), and $\bar{s} = 1$, $\bar{u} = \eta - 1$ for $q = -1$ ($\Phi = \pi$).

Remarkably, set (12) possesses a family of solutions with real s and complex u. To see it, we indicate that the equality $s - q\mathrm{Re}(u) = \eta$, being valid for an arbitrary ζ_0, holds true for any ζ. Transferring next to the absolute values and arguments of s and u, one can make sure that the conservation law $p_0 \equiv s^2/2 - q|u| = \mathrm{const}$ is valid for such solutions. It corresponds to a constant energy flux along the coordinate ζ. Employing this conservation law, we obtain a single second-order equation for s:

$$\ddot{s} = \eta - s(1 + p_0) + s^3/2. \tag{13}$$

This equation admits an obvious mechanical analogy with a unit-mass particle with coordinate $s(\zeta)$ moving in the potential $U(s) = -\eta s + (1 + p_0)s^2/2 - s^4/8$; ζ has to be treated as an effective time. For "initial" values $s_0 = s(0)$ and $\dot{s}_0 = \dot{s}(0)$, Eq. (13) enables one to find the "trajectory" $s(\zeta)$ for $\zeta \gtrless 0$. Note that the choice of the zero point of ζ is arbitrary.

The potential profile $U(\zeta)$ is generally different for different trajectories via the dependence of p_0 on s_0 and $\dot{s}_0$. The treatment is strongly simplified if we characterize each trajectory by its turning point s_0 corresponding to zero "velocity" $\dot{s}_0$. In this case, we have $p_0 = s_0^2/2 - q|\eta - s_0|$ according to Eq. (12) and, consequently, the potential profile $U = U(s, s_0)$ in an explicit form:

$$U = -\eta s + \frac{s^2}{2}\left(1 + \frac{s_0^2}{2} - q|\eta - s_0|\right) - \frac{s^4}{8}. \tag{14}$$

With this profile, one can find, analytically or numerically, trajectory $s(\zeta)$ for any s_0, η, and q.

A key point in our analysis of the localized and periodic solutions for $s(\zeta)$ is determination and classification of the turning points s_0 corresponding to maxima of $U(s, s_0)$. Equating to zero the derivative $\partial_s U(s, s_0)$ at $s = s_0$, we get the following: $qs_0|s_0 - \eta| - s_0 + \eta = 0$. Solutions of this equation for s_0 depend on $q = \mathrm{sgn}(\Delta_1\Delta_2)$.

For $q = 1$, there are three solutions for s_0. The first one, $s_0 = \bar{s}_- = 1$, is valid for $\eta \leqslant 1$. The corresponding profiles $U(s, 1, \eta)$ are illustrated by Fig. 4(a). The particle can move here between the right (shown by circles) and left turning

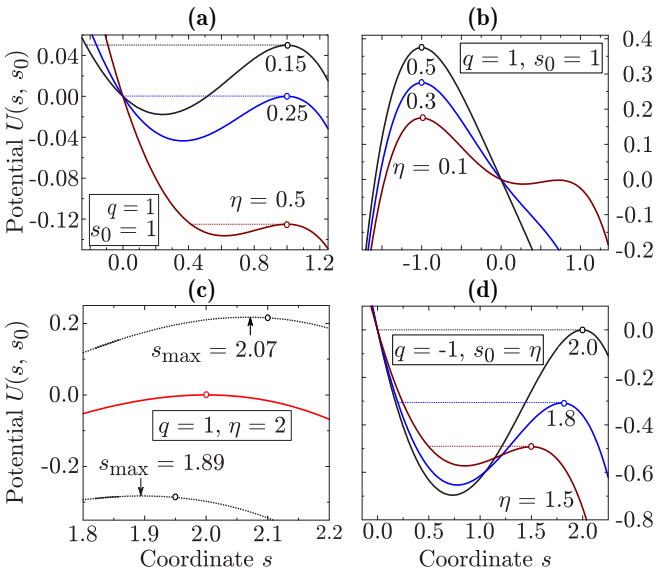

FIG. 4. Potentials $U(s, s_0)$ for different stopping points s_0 (circles) and values of η. (a)–(c) The cases $s_0 = 1$, -1, η for $q = 1$. (c) Shown also is the effect of small shifts of s_0 against η. (d) The case $s_0 = \eta > 1$ for $q = -1$. The horizontal dotted lines correspond to the soliton states.

points. A small decrease of s_0 changes $U(s, s_0)$ such that the particle oscillates periodically between two turning points, and the oscillation period tends to infinity for $s_0 \to 1$. For $s_0 > 1$, the regular solution breaks: The particle infinitely accelerates and $s(\zeta) \to \infty$. The second solution, $s_0 = \bar{s}_+ = -1$, is relevant to the potential profiles of Fig. 4(b). This case is not physical because solution $s(\zeta)$ breaks for any small deviation of s_0 from -1. For the third solution, $s_0 = \eta > 1$, any small deviations of s_0 against η change the potential such that the particle finds oneself to the right of the potential maxima [see Fig. 4(c)], leading to an infinite growth of $s(\zeta)$. Thus, only the first solution, where the value $s_0 = 1$ coincides with the background value $\bar{s}_-$, is physical for $q = 1$.

For $q = 1$, $s_0 = 1$, and $\eta < 1$, Eq. (12) admit an exact soliton solution:

$$s = \frac{\sqrt{\eta}\cosh(\zeta\sqrt{1-\eta}) + 2\eta - 1}{\sqrt{\eta}\cosh(\zeta\sqrt{1-\eta}) + 1},$$
$$f = \pm\sqrt{1-\eta}\,\frac{\sqrt{\eta}\sinh(\zeta\sqrt{1-\eta}) + i\sqrt{1-\eta}}{\sqrt{\eta}\cosh(\zeta\sqrt{1-\eta}) + 1}. \quad (15)$$

The normalized SH amplitude s is even in ζ, tends to the background value $\bar{s}_- = 1$ for $|\zeta| \to \infty$, and possesses the minimum value $2\sqrt{\eta} - 1$, that can be positive and negative depending on η. This solution corresponds to an infinitely long movement of the particle from the right turning point $s_0 = 1$ to the left turning point and back. The normalized complex FH amplitude f tends to opposite real values for $\zeta \to \pm\infty$, while $u = f^2$ tends to $u_- = 1 - \eta$. This means that $f(\zeta)$ is antiperiodic within the interval $[-\infty, \infty]$. Unless η is very close to 1, approaching the background values with increasing $|\zeta|$ occurs exponentially, i.e., very fast. For $\eta \to 1$, the soliton width tends to infinity. The soliton solution (15) has no limit for $\eta \to 0$: For $\eta \ll 1$, the values of $s(\zeta)$ and $u(\zeta)$ stay very close to the background values $\bar{s}_+ \simeq -1$, and $\bar{u}_+ \simeq -1$ within a finite range of $|\zeta|$ near 0 and tend exponentially to $\bar{s}_- \simeq \bar{u}_- \simeq 1$ for larger $|\zeta|$. With decreasing η, the left and right boundaries between these background regions shift to $\pm\infty$.

While the above soliton solution is valid, strictly speaking, only for an infinite range of ζ, it is of big value for finite ranges, provided that these ranges substantially exceed the soliton width. First, the difference between the peripheral values of s and f and the corresponding background values can be smaller than a natural noise level. Second, existence of soliton solutions ensures, as shown below, the presence of periodic solutions which are very close to the soliton ones.

To get periodic solutions for s and the corresponding solution for f, we employ the values s_0 slightly below 1. This is illustrated by Figs. 5(a) and 5(b).

Within the line width, the shape of each dip in Fig. 5(a) coincides with the soliton one. The difference is substantial only when $s(\zeta)$ and $f(\zeta)$ are very close to the background values 1 and $\sqrt{1-\eta} \simeq 0.837$, respectively. The π-step dependence of $\arg[f(\zeta)]$ is clearly seen; this shows that our solution satisfies the antiperiodic boundary conditions. The period ζ_0 depends on the deviation $\delta s_0 = s_0 - 1$ and tends to infinity for $\delta s_0 \to 1$. This allows one to adjust the period to the dimensionless resonator length $\zeta_R = 2\pi R|2\Delta_1 + \Delta_2|/|v_1 - v_2|$.

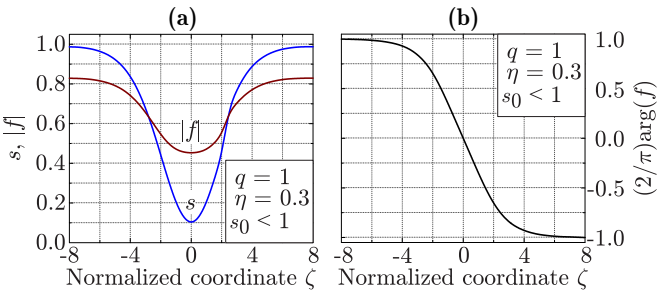

FIG. 5. Antiperiodic solitonlike solution for s and f at $q = 1$, $\eta = 0.3$, and $1 - s_0 \simeq 1.27 \times 10^{-2}$. The quantities s and $|f|$ are periodic with the period $\zeta_0 = 16$ (a), while the phase $\arg(f)$ changes by π within this period (b).

For sufficiently large values of ζ_R, periodic multisoliton solutions become possible.

Now we switch to the case $q = \mathrm{sgn}(\Delta_1\Delta_2) = -1$. Only the values $s_0 = \eta$ for $\eta > 1$, which correspond to $p_0 = \eta^2/2$, give here potential profiles with maxima at $s = s_0$. This is illustrated by Fig. 4(c). For each value $s_0 = \eta$, there is a left partner turning point providing the soliton state. In contrast to the case $q = 1$, $s_0 = \eta$, a small deviation $\delta s_0 = s_0 - \eta$ of any sign changes the potential $U(s, s_0)$ such that s_0 stays on the left of the potential maximum. In other words, there is a family of periodic states $s(\zeta)$ approaching the soliton state for $\delta s_0 \to 0$ regardless of the sign of δs_0. Note that the point $s_0 = \bar{s} = 1$, relevant to the spatially uniform background, corresponds to a minimum of $U(s, s_0)$; it is of no interest.

For $q = -1$, $s_0 = \eta$, and $\eta > 1$, Eq. (12) also admits an exact soliton solution:

$$s = \frac{\eta\cosh(a\zeta) - \eta^2 + 2}{\cosh(a\zeta) + \eta},$$
$$f = \pm\sqrt{2}a\,\frac{\sqrt{\eta+1}\cosh(a\zeta/2) - i\sqrt{\eta-1}\sinh(a\zeta/2)}{\cosh(a\zeta) + \eta}, \quad (16)$$

where $a = \sqrt{\eta^2 - 1}$. It corresponds to $s(0) = 2 - \eta < 1$, $s(\pm\infty) = \eta$, $f(0) = \pm\sqrt{2(\eta-1)}$, and $f(\pm\infty) = 0$. This soliton is thus SH dark and FH bright. Approaching the limiting values at $\pm\infty$ occurs exponentially. The localization scale substantially decreases with increasing η. Furthermore, the argument of f is an odd function of ζ, whose asymptotic values at $\pm\infty$ are below $\pi/4$ in the absolute value. Note also a useful link $|f|^2 = (\eta^2 - s^2)/2$. Further details on this soliton are given below in co-junction with an analysis of closely related solitonlike periodic states.

For $|\delta s_0| \ll 1$, we have solitonlike periodic solutions for $s(\zeta)$ and the corresponding solutions for $f(\zeta)$; they can be found numerically from Eqs. (12) or (13). The cases $\delta s_0 \lessgtr 0$ have not only similarities, but also important special features.

Figures 6(a) and 6(b) illustrate the case $\delta s_0 < 0$ for $\eta = 4$. Here the period of $s(\zeta)$ is $\zeta_0 = 6$. Within the line width, the curves $s(\zeta)$ and $|f(\zeta)|$ coincide with ones given by Eq. (16). The function $|f(\zeta)|$ has a characteristic two-hump structure. The tails ($|\zeta| > 2$), where the difference with the soliton is relatively large, are weak. In contrast to the case $q = 1$,

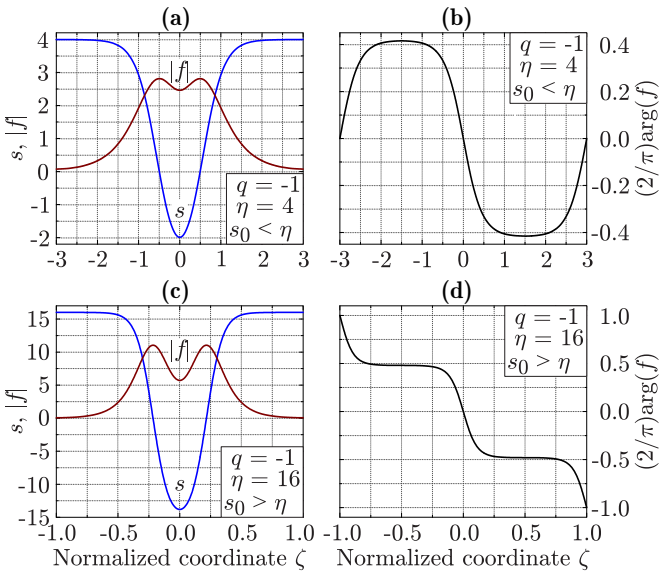

FIG. 6. Periodic solitonlike solutions for s, $|f|$, and $\arg(f)$ for $q = -1$ within one period; (a) and b) correspond to $\eta = 4$, $1 - s_0 \simeq 0.0035$, and to the period $\zeta_0 = 6$, while (c) and d) refer to $\eta = 16$, $1 - s_0 \simeq 0.005$, and $\zeta_0 = 2$. Note the difference in the horizontal and vertical scales between (a) and (b), and (c) and (d).

the function $\arg[f(\zeta)]$ is ζ_0 periodic; it experiences modest oscillations with ζ.

Figures 6(c) and 6(d) illustrate the case $\delta s_0 > 0$ for $\eta = 16$. Now, the period of $s(\zeta)$ and $|f(\zeta)|$ is $\zeta_0 = 2$, the vertical scale in Fig. 6(c) is enlarged compared to Fig. 6(a), and the tails of $s(\zeta)$ and $|f(\zeta)|$ are weakened. This effect of increasing η is relevant also to the case $\delta s_0 < 0$. The difference is in the behavior of $\arg[f(\zeta)]$, as shown in Fig. 6(d). This function is now steplike, so that the function $f(\zeta)$ is ζ_0 antiperiodic.

Regardless of the sign of δs_0, increasing $|\delta s_0|$ results in decreasing period ζ_0, broadening of the dips and peaks of $s(\zeta)$ and $|f(\zeta)|$, and in strengthening of the tails. The values of δs_0 are not necessarily small. The effect of increasing η is different. It is decreasing period ($\zeta_0 \propto 1/\eta$ for $\eta \gg 1$), narrowing of the dips and peaks, and suppression of the tails. In other words, the steady state tends to a periodic train of solitons with increasing η. The case of almost opposite Δ_2 and $2\Delta_1$ is unfavorable for solitons.

Requirements to the experimental parameters R, $\Delta_{1,2}$, and η, necessary to realize periodic solitonlike solutions, are different for the cases $q = 1$ and -1. In the case $q = 1$, when $\eta < 1$, the period ζ_0 cannot be smaller than 1, but is often ~10. Therefore, the dimension resonator length $\zeta_R = 2\pi R|2\Delta_1 + \Delta_2|/|v_1 - v_2|$ has to be much larger than 1. For $2\pi R \approx 1$ cm and $|\Delta_1| \approx |\Delta_2|$, this leads us to detunings $|\Delta_{1,2}| \gtrsim 10^9\ \mathrm{s}^{-1}$. The restriction from above $|\Delta_{1,2}| \ll \delta\omega = v_{1,2}/R \approx 10^{11}\ \mathrm{s}^{-1}$ can be easily fulfilled. In the case $q = -1$, when η can be much larger than 1, the period ζ_0 can be substantially smaller than 1. Here the detunings $|\Delta_{1,2}|$ can stay below $10^8\ \mathrm{s}^{-1}$. Keeping in mind that the decay constants $\gamma_{1,2}$ must be much smaller than $|\Delta_{1,2}|$, we see that substantially larger modal quality factors can be used.

The above theoretical treatments are relevant to the case $\gamma_{1,2} = v'_{1,2} = 0$. It is possible to get small corrections $\delta s(\tilde{\varphi})$ and $\delta f(\tilde{\varphi})$ to the above steady-state solutions within the linear approximation in small parameters γ_2 and $v'_{1,2}$. Such a linear perturbation approach [40] accounts for the degeneracy in the choice of position of the soliton center and is consistent with the known Fredholm alternative [41] for linear systems. However, the linear perturbation theory in γ_1 fails indicating a substantial modification of the initial soliton state. This means that more powerful perturbation techniques, like the Newton method (see [42] and references therein), have to be employed. Such a situation is not rare in the physics of solitons. In particular, it is known for Kerr solitons [42]. In our case, a strong effect of γ_1 on solitons is closely related to the strong effect on the spatially uniform background; see Fig. 6. Consideration of the impact of γ_1 on the soliton properties requires a separate study.

V. NUMERICAL SIMULATIONS

We investigated numerically stability of the found steady-state solutions within the modal approach relevant to ordinary differential equations (1) and, independently, within the slowly varying amplitude approach relevant to partial differential equations (4). The modal amplitudes $F_j(t)$ and $S_l(t)$ are linked to the 2π-periodic amplitudes $F(\varphi, t)$ and $S(\varphi, t)$ by the discrete Fourier transform. Both Eqs. (1) and (4) were solved in the time domain. As an initial condition for F_j, S_l, we used the inverse Fourier transform of a periodic solitonlike solution $F(\tilde{\varphi})$, $S(\tilde{\varphi})$ superimposed by very small random numbers δF_j, δS_l (modal noise). As initial conditions for $F(\varphi, t)$ and $S(\varphi, t)$, we employed $F(\tilde{\varphi})$, $S(\tilde{\varphi})$ superimposed by the Fourier transform of the modal noise. Different variants of periodic and antiperiodic initial conditions with $\Delta_1\Delta_2 \gtrless 0$ were used.

The number of points in the φ mesh and, correspondingly, the number of modes within each of the FH and SH frequency domains ranged from 512 to 2048. The nonlinear set of ordinary differential equations (1) was integrated using the fourth-order Runge-Kutta method with the time step ranging from 5×10^{-4} to 2×10^{-3} of the round-trip time R/c with $R = 1.59$ mm. The nonlinear partial differential equations for $F(\varphi, t)$ and $S(\varphi, t)$ were solved using the step-split Fourier method [43]; the step in time ranged from 5×10^{-6} to 2×10^{-5} of R/c. It was made sure that both methods gave essentially the same results and no real effect of time and φ steps was present. Also numerical solutions were checked in a series of limiting cases of initial conditions where the analytical solutions can be obtained easily.

Figure 7 exhibits representative results of our numerical simulations for an antiperiodic solitonlike solution relevant to $q = \mathrm{sgn}(\Delta_1\Delta_2) = 1$ and $\eta = 0.22$. Initially ($t < 10^{-8}$ s), the noise of $f_{\delta j}$ grows exponentially with an increment $\approx\Delta_{1,2}$ within a wide range of deviations $|\delta j|$; see Figs. 7(b) and 7(d). The normalized intensity dependencies $|f|^2(\tilde{\varphi})$ and $|s|^2(\tilde{\varphi})$ experience only minor changes at this stage, and the FH and SH intensity patterns move practically with the same velocity v_0; see Figs. 7(a) and 7(b). For larger times, distortions of the steady-state solution become substantial, the notion of a common velocity fails, and a strong fragmentation of both patterns in $\tilde{\varphi}$ takes place [see Fig. 7(e)]. At the same time, both FH and SH patterns remain spatially coherent and

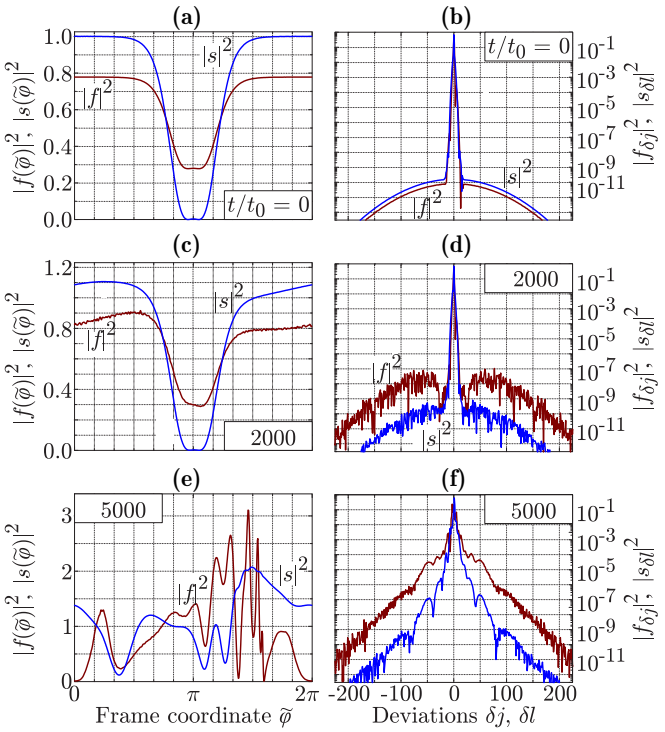

FIG. 7. Numerical results on stability of the antiperiodic solitonlike solution with $q = 1$ and $\eta = 0.22$ ($2\pi R = 1$ cm, $\Delta_1 = \Delta_2 = 3 \times 10^9$ s^{-1}, $v_1 - v_2 = 10^{-2}c$, $\gamma_{1,2} = 0$, and $v'_{1,2} = 0$). The time t is normalized to $t_0 = R/c \simeq 5 \times 10^{-12}$ s. The left column shows the normalized intensities $|f|^2$ and $|s|^2$ versus φ and the right column shows the normalized modal powers $|f_{\delta j}|^2$ and $|s_{\delta j}|^2$ versus the deviations of the modal numbers $\delta j = j - j_0$ and $\delta l = l - l_0$.

substantially exceeding the noise level. The spectral broadening is continuing [see Fig. 7(d)]. All this evidences that the antiperiodic solution with $F \neq 0$ is preferable for the system as compared to the allowed and stable solution with $F = 0$ and $S \neq 0$; see also Fig. 3.

Changes of the simulation and external parameters, switching from the antiperiodic to periodic solutions and to the case $q = -1$, inclusion of nonzero $\gamma_{1,2}$ and $v'_{1,2}$ result in modification of details, but the fact of instability remains unchanged. At the same time, solutions with a zero noise stay unchanged indefinitely long; this confirms correctness of the simulations.

Finally, we stress that the above numerical analysis refers to the soliton solutions calculated at $\gamma_{1,2} = 0$ and $v'_{1,2} = 0$. A strong impact of γ_1 on the soliton shape can bring the system to stability by analogy with Kerr solitons [42].

VI. DISCUSSION

While the differences between our $\chi^{(2)}$ case and the case of $\chi^{(3)}$ combs are quite evident, distinctions from the known analyses of $\chi^{(2)}$ solitons have to be considered. The former results were relevant mostly to the conservative case (zero pumping and dissipation) and infinite media [17]. A considerable part of theoretical considerations was relevant to the spatial solitons, which are essentially different from the temporal solitons. Applications to microresonators, including discreteness of the modal structure, practicability of the chosen parameters, and the possibilities of pumping were not considered. Three recent papers on dissipative solitons in microresonators [18–20] are relevant to FH pumping at the point of equal group velocities, $v_1(\lambda_p) = v_2(\lambda_p)$.

Each of the general assumptions—single-mode approximation and perfect radial poling—is rather obligatory. Often, there are plenty of competing modes characterized not only by the azimuth number, but also the radial and polar numbers [1,44,45]. It is unlikely that accounting for these modes can be compatible with analysis of coherent solitonlike states. Suppression of undesirable modes in high-Q resonators is a serious technological task that requires special efforts [46–48]. Radial poling is generally imperfect because of off-centering of the domain structure [27]. This leads to the presence of a few (or several) Fourier peaks of the quadratic susceptibility coefficient, separated by the intermodal distance, instead of a single N peak in Fig. 1(d). Unless only one of these peaks is dominating, equations for slowly varying amplitudes $F(\varphi, t)$ and $S(\varphi, t)$ can fail. The use of the linear poling [49], leading to broad Fourier spectra of the quadratic susceptibility, is, most probably, very harmful for coherent solutions.

A substantial difference of the group velocities for the first and second harmonics is a generic feature of $\chi^{(2)}$ microresonators. For many resonators, the difference $|v_1 - v_2|$ can be estimated as $\sim 10^{-2}c = 3 \times 10^8$ cm/s within broad spectral ranges of the pump wavelength λ_p. Any steady-state comb solution $F(\varphi - v_0 t)$, $S(\varphi - v_0 t)$ implies that the difference between v_1 and v_2 is compensated by the quadratic nonlinearity. This compensation is fundamentally different from the known compensation between dispersion and nonlinearity for cubic solitons. Determination of coherent steady-state solutions with nonlinearly compensated velocity difference is by itself a big challenge. Above we have found two big families of such localized soliton solutions. The effects of dispersion can be estimated here as secondary for not extremely narrow FH and SH solitons. Specifically, they are weak until the comb spectrum consists of $\sim 10^3$ (or less) frequency peaks.

Indeed, the velocity difference can be suppressed when working at the point $v_1(\lambda_p) = v_2(\lambda_p)$. In this case, the situation becomes similar to that typical of $\chi^{(3)}$ combs. However, the question about the effect of inevitably present relatively small velocity differences remains open.

A surprising feature of the found nonlinear regimes is the presence of two entirely different types of spatial symmetry in the case of SH pumping, 2π-periodic and -antiperiodic solutions. While the total electromagnetic fields are ultimately 2π periodic, these solutions are topologically different. In particular, the antiperiodic solutions have no spatially uniform backgrounds. Both periodic and antiperiodic solitons admit simple analytical representations which are new to the best of our knowledge. Furthermore, each soliton is associated with a family of solitonlike periodic states with adjustable spatial periods.

Finding of big families of periodic and antiperiodic soliton solutions caused by a large group-velocity difference can be regarded as a significant step in realization of $\chi^{(2)}$ frequency combs. These solutions are relevant to the situations which are the most typical for $\chi^{(2)}$ microresonators. Similar

findings are followed usually by more special studies relevant to the effects of secondary parameters. While the "naked" solitons with $\gamma_{1,2} = v'_{1,2} = 0$ show an instability against small perturbations, it is quite possible that "γ_1 dressing" of these localized states will provide the necessary stabilization by analogy with the Kerr solitons. This issue requires further studies. By analogy with finding of new solutions of the lossless LL equation [39], one can expect emergence of new walk-off controlled $\chi^{(2)}$ comb solutions.

VII. CONCLUSIONS

We have derived and analyzed coupled nonlinear equations for FH and SH envelopes relevant to the frequency comb generation in $\chi^{(2)}$ microresonators. They incorporate selective SH pumping, quasi-phase-matching via radial poling, different group velocities and frequency dispersions, and the modal decay. Within a broad range of parameters, the effect of the group velocity difference is found to be crucial for comb-related solutions. It is shown that, depending on the pump frequency, solutions for the modal envelopes can be topologically different and relevant to periodic and antiperiodic boundary conditions. Within a basic model disregarding the effects of weak dispersion and modal decay, we have found analytically and numerically two families of steady-state soliton and solitonlike solutions. These solutions correspond to the FH and SH envelopes moving with the same velocity without shape changes and possessing equidistant frequency spectra; they can be both periodic and antiperiodic. Analytical and numerical calculations show, nevertheless, that stability of the analytical comb solutions cannot be ensured without account for an impact of the small FH dissipative constant on the soliton shape.

ACKNOWLEDGMENT

The work of S.S. was supported by the Russian Foundation for Basic Research (Project No. 18-29-20025).

[1] K. J. Vahala, Optical microcavities, Nature (London) **424**, 839 (2003).

[2] L. Maleki, V. S. Ilchenko, A. A. Savchenkov, and A. B. Matsko, Crystalline whispering gallery mode resonators in optics and photonics, in *Practical Applications of Microresonators in Optics and Photonics*, edited by A. B. Matsko (CRC Press, Boca Raton, 2009).

[3] A. B. Matsko and V. S. Ilchenko, Optical resonators with whispering-gallery modes, Part I: Basics, IEEE J. Sel. Top. Quantum Electron. **12**, 3 (2006).

[4] V. S. Ilchenko and A. B. Matsko, Optical resonators with whispering-gallery modes, Part II: Applications, IEEE J. Sel. Top. Quantum Electron. **12**, 15 (2006).

[5] D. Strekalov, Ch. Marquardt, A. Matsko, H. Schwefel, and G. Leuchs, Nonlinear and quantum optics with whispering gallery resonators, J. Opt. **18**, 123002 (2016).

[6] P. Del'Haye *et al.*, Optical frequency comb generation from a monolitic microresonator, Nature (London) **450**, 1214 (2007).

[7] P. Del'Haye *et al.*, Octave Spanning Tunable Frequency Comb from a Microresonator, Phys. Rev. Lett. **107**, 063901 (2011).

[8] T. J. Kippenberg, R. Holzwarth, and S. A. Diddams, Microresonator based optical frequency combs, Science **332**, 555 (2011).

[9] T. Herr *et al.*, Universal formation dynamics and noise of Kerr-frequency combs in microresonators, Nat. Photon. **6**, 480 (2012).

[10] Y. K. Chembo and C. R. Menyuk, Spatiotemporal Lugiato-Lefever formalism for Kerr-comb generation in whispering gallery-mode resonators, Phys. Rev. A **87**, 053852 (2013).

[11] T. Herr *et al.*, Temporal solitons in optical microresonators, Nat. Photon. **8**, 145 (2014).

[12] X. Yi, Q.-F. Yang, M.-J. Suh, and K. Vahala, Soliton frequency comb at microwave rates in a high-Q silica microresonator, Optica **2**, 1078 (2015).

[13] Y. K. Chembo, Kerr optical frequency combs: Theory, applications and perspectives, Nanophotonics **5**, 214 (2016).

[14] M. G. Suh and K. Vahala, Gigahertz-repetition-rate soliton microcombs, Optica **5**, 65 (2018).

[15] T. J. Kippenberg, A. L. Gaeta, M. Lipson, and M. L. Gorodetsky, Dissipative Kerr solitons in optical microresonators, Science **361**, 567 (2018).

[16] N. Akhmediev and A. Ankiewicz, *Dissipative Solitons*, Lecture Notes in Physics (Springer-Verlag, Berlin/Heidelberg, 2005).

[17] A. V. Buryak, P. Di Trapani, D. V. Skryabin, and S. Trillod, Optical solitons due to quadratic nonlinearities: From basic physics to futuristic applications, Phys. Rep. **370**, 63 (2002).

[18] T. Hannson, P. Parra-Rivas, M. Bernard, F. Leo, L. Gelens, and S. Wabnitz, Quadratic sioliton combs in doubly resonant second-harmonic generation, Opt. Lett. **43**, 6033 (2018).

[19] A. Villois and D. Skryabin, Soliton and quasi-soliton frequency combs due to second harmonic generation in microresonators, Opt. Express **27**, 7098 (2019).

[20] A. Villois *et al.*, Frequency combs in a microring optical parametric oscillator, Opt. Lett. **44**, 4443 (2019).

[21] V. Ulvila, C. R. Phillips, L. Halonen, and M. Vainio, High-power mid-infrared frequency comb from a continuous-wave-pumped bulk optical parametric oscillator, Opt. Express **22**, 10535 (2014).

[22] F. Leo *et al.*, Walk-off-Induced Modulation Instability, Temporal Pattern Formation, and Frequency Comb Generation in Cavity-Enhanced Second-Harmonic Generation, Phys. Rev. Lett. **116**, 033901 (2016).

[23] S. Mosca *et al.*, Direct generation of optical frequency combs in $\chi^{(2)}$ nonlinear cavities, Nanophotonics **5**, 316 (2016).

[24] S. Mosca *et al.*, Modulation Instability Induced Frequency Comb Generation in a Continuously Pumped Optical Parametric Oscillator, Phys. Rev. Lett. **121**, 093903 (2018).

[25] P. Parra-Rivas *et al.*, Frequency comb generation through the locking of domain walls in doubly resonant dispersive optical parametric oscillators, Opt. Lett. **44**, 2004 (2019).

[26] M. Jankowski, A. Marandi, C. R. Phillips, R. Hamerly, K. A. Ingold, R. L. Byer, and M. M. Fejer, Temporal Simultons in Optical Parametric Oscillators, Phys. Rev. Lett. **120**, 053904 (2018).

[27] T. Beckmann *et al.*, Highly Tunable Low-Threshold Optical Parametric Oscillation in Radially Poled Whispering Gallery Resonators, Phys. Rev. Lett. **106**, 143903 (2011).
[28] M. Mohageg *et al.*, Calligraphic poling of lithium niobate, Opt. Express **13**, 3408 (2005).
[29] M. Gorodetsky and A. Fomin, Geometrical theory of whispering-gallery modes, IEEE J. Sel. Top. Quantum Electron. **12**, 33 (2006).
[30] M. L. Gorodetsky and Y. A. Demchenko, Accurate analytical estimates of eigenfrequencies and dispersion in whipering-gallery spheroidal resonators, Proc. SPIE **8236**, 823623 (2012).
[31] B. Sturman, E. Podivilov, C. S. Werner, and I. Breunig, Vectorial perturbation theory for axisymmetric whispering gallery resonators, Phys. Rev. A **99**, 013810 (2019).
[32] D. N. Nikogosyan, *Nonlinear Optical Crystals: A Complete Survey* (Springer, Berlin, 2005).
[33] B. Sturman and I. Breunig, Generic description of second-order nonlinear phenomena in whispering-gallery resonators, J. Opt. Soc. Am. B **28**, 2465 (2011).
[34] J. U. Fürst *et al.*, Naturally Phase-Matched Second-Harmonic Generation in a Whispering-Gallery-Mode Resonator, Phys. Rev. Lett. **104**, 153901 (2010).
[35] U. Schlarb and K. Betzler, A generalized Sellmeier equation for the refractive indices of lithium niobate, Ferroelectrics **156**, 99 (1993).
[36] D. E. Zelmon, D. L. Small, and D. Jundt, Infrared corrected Sellmeier coefficients for congruently grown lithium niobate and 5 mol. magnesium oxide-doped lithium niobate, J. Opt. Soc. Am. B **14**, 3319 (1997).
[37] L. A. Lugiato and R. Lefever, Spatial Dissipative Structures in Passive Optical Systems, Phys. Rev. Lett. **58**, 2209 (1987).
[38] S. Coen, H. G. Randle, T. Sylvestre, and M. Erkintalo, Modeling of octave-spanning Kerr frequency combs using a generalized mean-field Lugiato-Lefever model, Opt. Lett. **38**, 37 (2013).
[39] W. H. Renninger and P. T. Rakich, Closed-form solutions and scaling laws for Kerr frequency combs, Sci. Rep. **6**, 24742 (2016).
[40] E. A. Kuznetsov and F. Dias, Bifurcations of solitons and their stability, Phys. Rep. **507**, 43 (2011).
[41] J. Matheus and R. L. Walker, *Mathematical Methods of Physics*, 2nd ed. (W. A. Benjamin, New York, 1970).
[42] I. V. Barashenkov and Yu. S. Smirnov, Existence and stability chart for the ac-driven, damped nonlinear Schrödinger solitons, Phys. Rev. E **54**, 5707 (1996).
[43] R. A. Fisher and W. K. Bischel, Numerical studies of the interplay between self-phase modulation and dispersion for intense plane-wave laser pulses, J. Appl. Phys. **45**, 4921 (1975).
[44] I. Breunig *et al.*, Whispering gallery modes at the rim of an axisymmetric optical resonator: Analytical versus numerical description and comparison with experiment, Opt. Express **21**, 30683 (2013).
[45] G. Schunk *et al.*, Identifying modes of large whispering-gallery mode resonators from the spectrum and emission pattern, Opt. Express **22**, 30795 (2014).
[46] A. Guarino *et al.*, Electrooptically tunable microring resonators in lithium niobate, Nat. Photon. **1**, 407 (2007).
[47] S. Y. Siew, S. S. Saha, M. Tsang, and A. J. Danner, Rib microring resonators in lithium niobate on insulator, IEEE Photon. Technol. Lett. **28**, 573 (2016).
[48] R. Wolf, I. Breunig, H. Zappe, and K. Buse, Cascaded second-order optical nonlinearities in on-chip micro rings, Opt. Express **25**, 29927 (2017).
[49] V. S. Ilchenko, A. A. Savchenkov, A. B. Matsko, and L. Maleki, Nonlinear Optics and Crystalline Whispering Gallery Mode Cavities, Phys. Rev. Lett. **92**, 043903 (2004).